Bismuth oxysulfide thin films for light and humidity sensing

A.V. Mazanik[1*], I.A. Svito[1], V.K. Ksenevich[2], E.A. Bondarenko[3],
L.S. Khoroshko[1], A.I. Kulak[4], E.A. Streltsov[5]

[1] Department of Solid State Physics and Nanotechnologies, Faculty of Physics, Belarusian State University, 4, Nezavisimosti Av., 220030 Minsk, Republic of Belarus;
[2] Department of Semiconductor Physics and Nanoelectronics, Faculty of Physics, Belarusian State University, 4, Nezavisimosti Av., 220030 Minsk, Republic of Belarus;
[3] Department of Physical Chemistry and Technology of Polymers, Faculty of Chemistry, Silesian University of Technology, Strzody 9, 44-100 Gliwice, Poland;
[4] Institute of General and Inorganic Chemistry, National Academy of Sciences of Belarus, Surganov St. 9/1, 220072 Minsk, Republic of Belarus;
[5] Electrochemistry Department, Faculty of Chemistry, Belarusian State University, 4, Nezavisimosti Av., 220030 Minsk, Republic of Belarus;
[*] Corresponding author: mazanikalexander@gmail.com.

Highlights

- bismuth oxysulfide films have high sensitivity to changes of relative humidity;
- this is originated from nanoplate-like structure of the films;
- water adsorption leads to ionic conductivity and electron acceptance from film.

Abstract

Bismuth oxysulfide (BOS) films formed on dielectric glass substrate by the chemical bath deposition have a high sensitivity to moisture content demonstrating decrease of the electrical resistance up to three orders of magnitude when the relative humidity (RH) increases from 5 to 85%. High sensitivity of resistive structure representing 0.65 μm thick film between two Ag contacts is associated with peculiarities of its microstructure. BOS films are composed of randomly oriented thin plate crystals. The presence of a great number of intergrain boundaries restricts transport of charge carriers (both in the dark and under illumination), which is desirable for resistive humidity sensors. As BOS films possess a high surface-to-volume ratio, this makes them ultra-sensitive to adsorption of various molecules and, in particular, water. It is supposed that ionic conductivity in a thin film of adsorbed water plays a crucial role in fast response of sensor (1–3 s) to adsorption-desorption cycles.

Keywords

Bismuth oxysulfide; heat treatment; resistance; photoconductivity; humidity; sensing.

1. Introduction

Nowadays, there is a growing interest in the development of photodetectors based on nanostructured semiconductor bismuth compounds (sulfide Bi_2S_3 [1–8], oxysulfides of various compositions ($Bi_9O_{7.5}O_6$, Bi_2O_2S) [9, 10], thioiodide BiSI [11], selenoiodide BiSeI [12], oxyiodide BiOI [13, 14]). However, the sensitivity of such devices as a rule is rather poor making important their further improvement, as well as looking for new materials for production of detectors. The aforenamed sensors can be divided into two groups. In the first case, a solid-state structure – a photoresistor – is formed, in which the current flows in the plane of the film. The second approach is based on formation of a photoelectrochemical structure, when an absorbing semiconductor layer is in contact with an electrolyte, and the current flows in the direction normal to the film plane. It is obvious that solid-state structures are much more convenient from the point of view of their practical applications; however, when using them, a problem associated with the scattering and recombination of charge carriers at the boundaries between the particles forming the film (nanobelts, nanoplates, etc.) may arise.

Another interesting application of oxide and chalcogenide semiconductors and, in particular, bismuth compounds is associated with creation of devices for relative humidity sensing [15–19]. One of the simplest types of RH sensors is resistive, where resistance changes under variation of RH value [20–21]. Despite the difference in mechanisms of interaction of water molecules with the surface of various materials and, correspondingly, the difference in response to RH changes, it is obvious that a high surface-to-volume ratio is desirable for high device sensitivity. In this connection, nanostructured materials (arrays of nanowires, nanobelts, nanoplates, etc.) are of heightened interest.

Recently, a new semiconductor material – bismuth oxysulfide (BOS) $Bi_{10}O_6S_9$ has been synthesized [22–24]. Photoelectrochemical properties of BOS were investigated in details, and in particular a great photoconductivity under electrochemical polarization in various aqueous electrolytes was discovered [22]. The films of bismuth oxysulfide are composed of thin (a few tens of nanometers) randomly oriented plate crystals and have the energy gap of 1.4 eV [22]. Such pronounced platelet-like structure provides a high surface-to-volume ratio allowing considering this material as promising for sensor applications, whereas the above-mentioned band gap energy value points to the possibility to use this material for detection of visible light. However, the use of electrolytes (first of all, aqueous) makes significant demands on the corrosion and photocorrosion hardness of semiconductor electrodes, on the hermeticity of an electrochemical cell and a fire safety (when organic solvents are used).

In this work, we study the basic solid state ("dry") electrical properties of BOS films in the dark and under illumination, as well as the influence of heat treatment on these properties. A possibility to prepare light and humidity sensors based on the bismuth oxysulfide films is analyzed.

2. Experimental

BOS films were prepared by the chemical bath deposition onto dielectric glass substrates according to the method described in details in [22]. The aqueous solutions for deposition contained 0.021 M $Bi(NO_3)_3$, 0.73 M triethanolamine, 0.21 M thiourea and 0.16 M NH_3 and was heated on the boiling water bath. Deposition time was equal to 80 min.

For in-plane electrical measurements, two parallel contacts were formed on the film surface using a silver paste. Intercontact distance was equal to 0.3 mm. Evaluation of electrical properties of the prepared BOS films was carried out by the measurement of their current-voltage (I-V) curves using a Keithley 2400 source-meter in the dark and under illumination. Three monochromatic ProLight PM6B-3LFx LEDs (wavelength 465, 525, or 623 nm, which corresponds to the band-to-band light absorption) equipped with quartz condenser lens with variable intensity were used in these experiments. A calibrated Hamamatsu 1336 8BQ photodiode was used for determination of the incident light intensity. The maximal illumination intensity was equal to 32 mW/cm^2 for the LED emitting at the wavelength of 465 nm.

The films were subjected to a vacuum heat treatment at 200 ^{o}C. Such temperature was chosen because it was established earlier that the heat treatments of the films at higher temperatures modify their phase composition [22].

The phase composition of the BOS films was controlled by the X-ray diffraction (XRD) and Raman spectroscopy. XRD analysis was carried out with an Empyrean diffractometer (PANalytical; Cu K_α source with a Ni-filter, 0.01 degree step). Raman spectroscopy was performed using a Nanofinder HE (LOTIS-TII) confocal spectrometer [25–27]. In these experiments, a CW laser (532 nm) was used for the excitation with intensity of incident light attenuated down to 60 μm to avoid a sample damage.

Thermogravimetric (TG) analysis was performed in argon atmosphere at a scanning rate of 5 °C/min with a NETZSCH STA 409 PC/PG analyzer in the temperature range of 25–200 °C.

The processes of adsorption-desorption of water vapor on the surface of the films were studied at room temperature in a darkened climate chamber. The film was connected to a Keithley 2450 source-meter. The pressure of the residual gases was less than 0.1 mbar. Cyclic processes of adsorption and desorption of water vapor on the surface of the samples were realized by puffing saturated water vapor into the chamber and then pumping it out using a forepump. Since the films have a certain persisted photoconductivity, they were kept in the dark for half an hour before the start of the experiment. Then a constant voltage of 20 V was applied to the film, and the dependence of the current on time

(chronoamperogram) was recorded. Simultaneously with the current, the relative humidity in the chamber was controlled using a SHT75 humidity and temperature sensor (Sensirion).

3. Results and Discussion

3.1. Structural properties of BOS films

Figures 1a–1c demonstrate typical scanning electron microscopy images for the as-prepared BOS film. As is seen from Figs. 1a and 1b, the film is composed of randomly oriented thin plates and has very friable (non-dense) structure. According to Fig. 1c, the film has uniform thickness of appr. 0.65 μm. XRD, Raman spectroscopy and TG analyses of the BOS films will be discussed further.

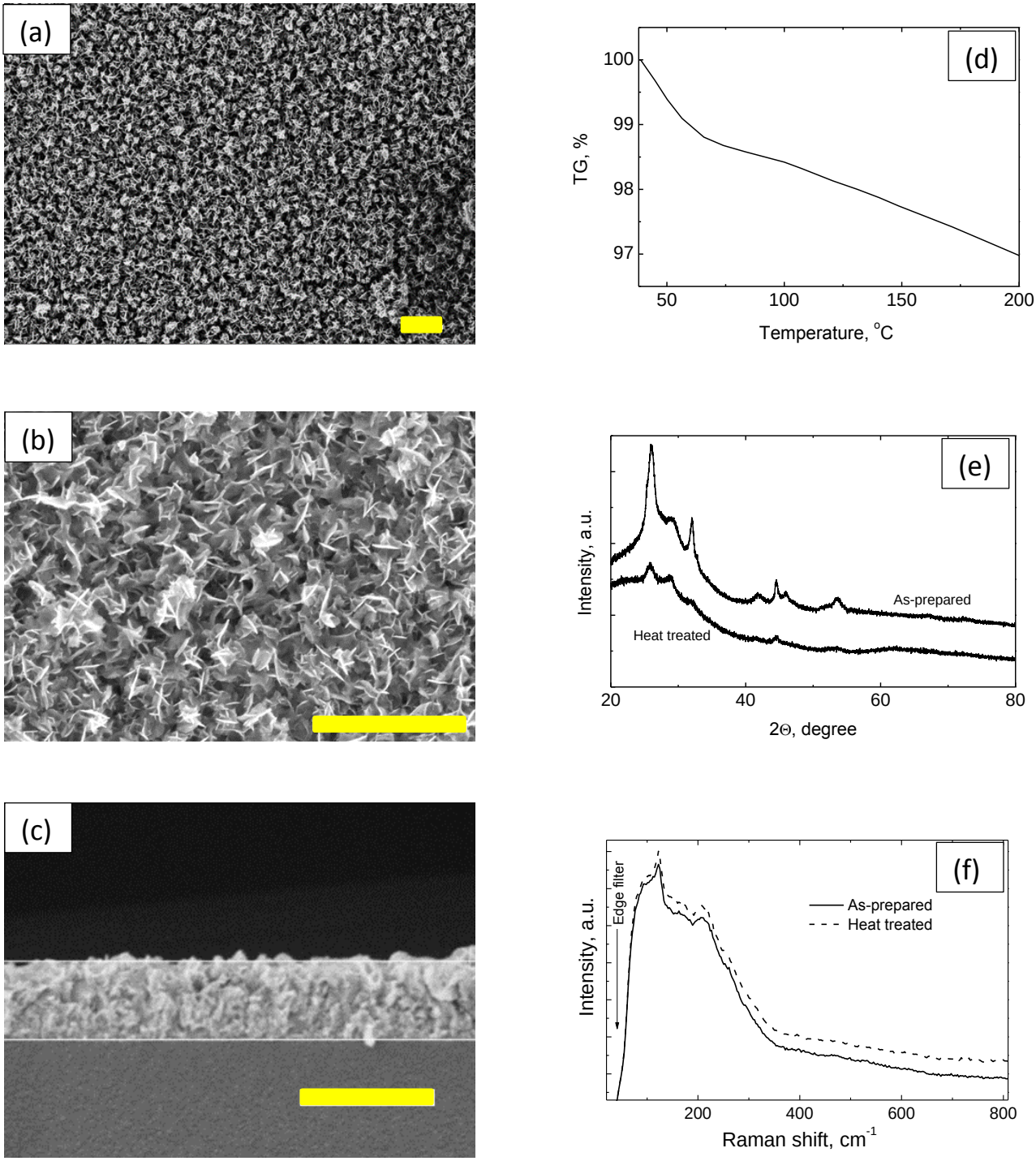

Fig. 1. Scanning electron microscopy images of the as-prepared BOS film in in-plane (a, b) and cross-sectional (c) geometries, scale bars corresponds to 1 μm; TG curve of BOS (d); XRD patterns (e) and Raman spectra (f) of BOS film before and after heat treatment at 200 °C.

3.2. Electrical properties of the as-prepared films

The experiments have demonstrated the linearity of the dark I-V curves of the as-prepared BOS films. The resistivity calculated from the dark I-V curves was estimated about $3 \cdot 10^5$ Ω·cm, and such high dark resistance is desirable for formation of photosensors. The observed high resistivity value seems to be originated from a great number of the interfaces between plate crystals, where existence of potential barriers impeding charge transfer is expected.

High resistivity of the as-prepared films did not allow reliable determining the sign of their thermal voltage; however, as it was revealed previously from electrochemical measurements [22], the films possess *n*-type conductivity.

In Fig. 2, the variation of the current between two Ag contacts formed on the surface of the BOS film under step-wise variation of the incident light intensity and under a constant bias voltage of 50 V is presented. As is seen, the films reveal photoconductivity under visible light illumination. Moreover, one can see long-time relaxations of the current after switch-off of the light (persistent photoconductivity), which is inherent to disordered semiconductors. From the kinetics of the current change given in Fig. 2, lux-ampere curves were plotted (dependence of the current increment under illumination normalized to the dark current on the incident light intensity, Fig. 3).

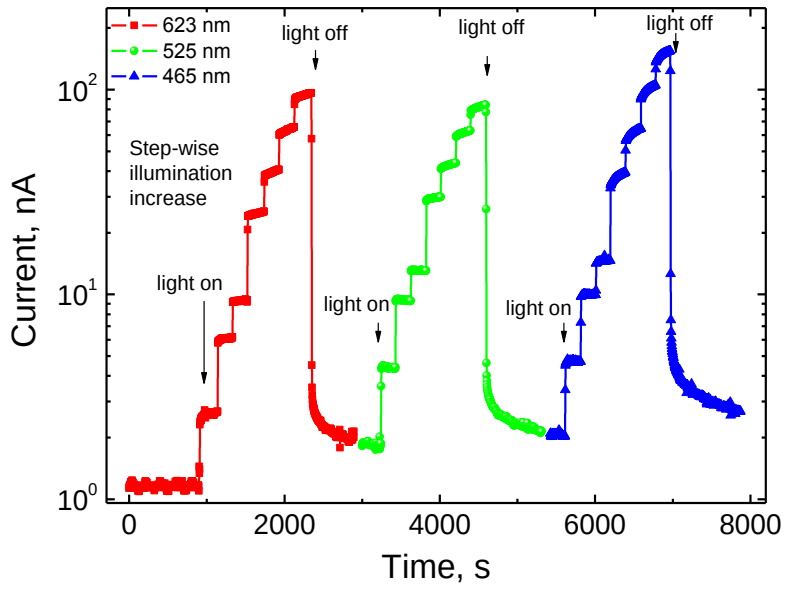

Fig. 2. Kinetics of the current changes of the as-prepared BOS film under step-wise variation of incident light intensity.

The obtained lux-ampere curves can be fitted well by the power-like function

$$\frac{I - I_{dark}}{I_{dark}} = CS^n \quad , \tag{1}$$

where I is the current under illumination, I_{dark} is the dark current, S is the intensity of the incident light, and C is the constant. The values of exponent n vary from 0.62 to 0.7 depending on the wavelength, which indicates an intermediate case between quadratic (n = 0.5) and linear (n = 1) recombination.

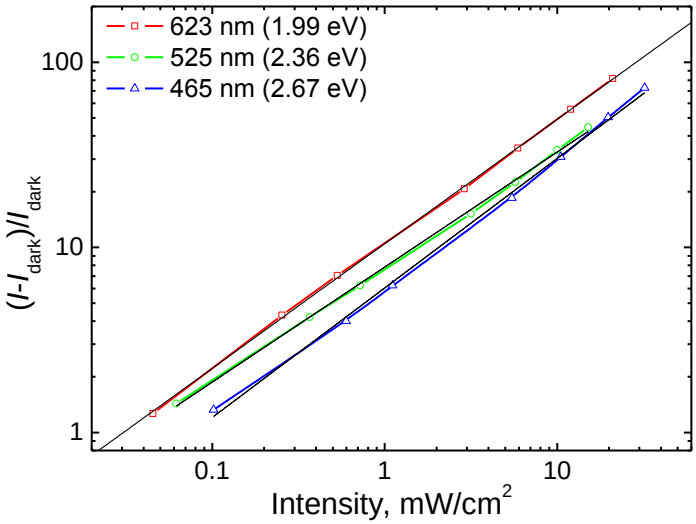

Fig. 3. Lux-ampere curves for the as-prepared BOS film derived from dependences given in Fig. 2.

Taking into account the geometrical size of the studied films, as well as the intensity of the incident light, the external quantum efficiency (EQE) was estimated to be equal to appr. 0.2%. This is significantly lower in comparison with the EQE values for processes in electrolytes (up to 2500%) [22]. The observed difference can be explained by the different geometry of current passing. In the photoelectrochemical experiments, the current passes across to the film, whereas in this work, the in-plane geometry was applied. As is known, in the case of the fundamental light absorption, the photocurrent density j_{ph} can be represented as

$$j_{ph} = j - j_{dark} = (\sigma - \sigma_{dark})E = e(\mu_n + \mu_p)\Delta nE = e(\mu_n + \mu_p)\tau gE \quad , \qquad (2)$$

where j and j_{dark} are the current densities under illumination and in the dark, respectively; σ and σ_{dark} are the conductivities of the film under illumination and in the dark, respectively; E is the electric field strength; e is the electron charge; Δn is the photoinduced increase in the concentration of electron-hole pairs; μ_n and μ_p are the mobilities of electrons and holes, respectively, τ is the lifetime of charge carriers, and g is the rate of their photogeneration. In the case of electrochemical measurements, $E \approx 10^6$ V/m (the voltage drop in the film $U \approx 1$ V, and the film thickness $d \approx 1$ um). In the case of in-plane measurements, $E \approx 1.7 \cdot 10^5$ V/m (the voltage drop in the film $U \approx 50$ V, and the intercontact distance $d \approx 0.3$ mm).

The second reason of the significant difference in EQE values for solid state and electrochemical measurements is related to the different impact of boundaries between the nanoplates. In electrochemical experiments, each plate has a contact with electrolyte; the length of path of charge carriers in semiconductor does not exceed the film thickness and, correspondingly, the contribution of their recombination and scattering at the boundaries between nanoplates is insignificant. On the contrary, in the case of in-plane experiments, the intercontact distance (a hundreds of micrometers) is significantly larger in comparison with the linear size of plates (about micrometer) resulting in pronounced influence of interface recombination and scattering on the observed photoelectrical properties. According to the light induced transient grating method [28–30], the diffusion coefficient of charge carriers in the BOS films does not exceed 0.01 cm^2/s, whereas their lifetime equals to a few tens of picoseconds [23]. Interface recombination results in reduction of non-equilibrium concentration of charge carriers under steady-state illumination, and their scattering at the inter-particle interfaces leads to the decrease of their mobility.

3.3. Influence of heat treatment on the electrical properties of the BOS films

As is seen from Fig. 4, the increase of temperature gives rise to the increase of electrical conductivity with a variable activation energy. In the temperature range 300–350 K close to the room temperature (marked with vertical dash lines in Fig. 4b), the activation energy equals to 0.13 eV. Note that heat treatment at 200 °C leads to decrease of resistance by appr. 7 orders of magnitude. However, the long-time (a few month) storage of the heat treated films in the dark at the atmosphere results in nearly full recovery of their resistance.

We assume that during vacuum annealing, a part of the oxygen and sulfur atoms are removed from the films, and the arising anion vacancies act as donor centers. This argumentation is supported by the TG analysis (Fig. 1d). As is seen, in the studied temperature range, there are two regions with different slopes on the TG curve. It is reasonable to associate the low-temperature region (below appr. 70 °C) with the water desorption, whereas at higher temperatures the mass loss is determined mainly by removal of atoms from the anion sublattice. The increase of the donor concentration results in a decrease in the height of potential barriers Φ at the interfaces between the nanoplates according to the well-known relation [31]

$$\Phi = \frac{e^2 N_S^2}{8\varepsilon_0 \varepsilon N_d} \quad , \tag{3}$$

where N_S is the surface density of the charged electronic states at the interface, ε_0 is the electric constant, ε is the permittivity of semiconductor, and N_d is the concentration of ionized donors in BOS semiconductor. Decrease of the potential barriers' height, in turn, reduces the film resistance. During the storage of the films in air after heat treatment, atmospheric oxygen is captured by them, which gives rise to a decrease in the concentration of vacancies and, correspondingly, to slow recovery of the film resistance.

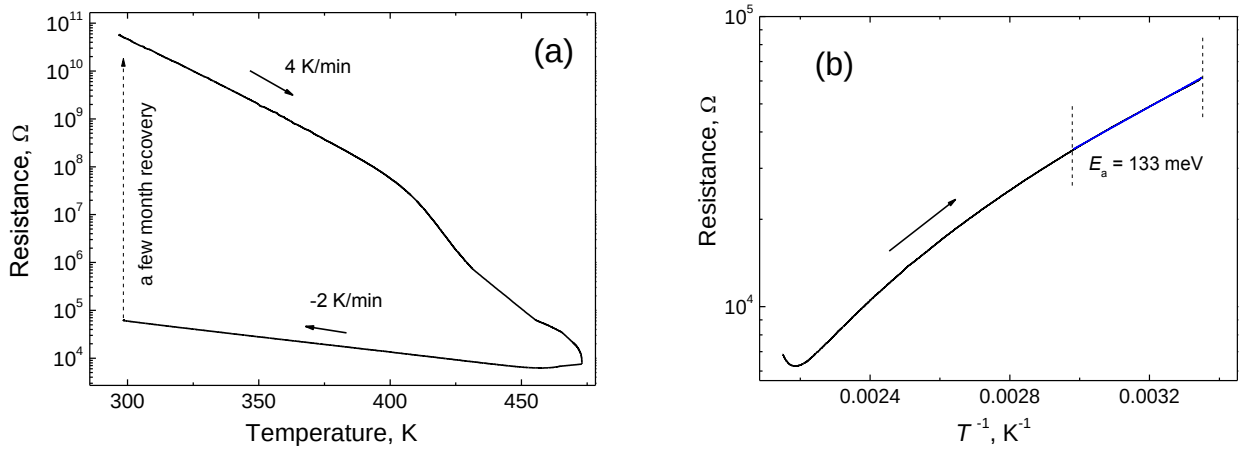

Fig. 4. Temperature dependence of BOS film resistance during vacuum heat treatment in the linear-log (a) and Arrhenius (b) coordinates.

Measurement of thermal voltage demonstrates *n*-type conductivity of the BOS films after vacuum heat treatment, which is in agreement with their electrochemical behavior [22].

Both XRD and Raman spectroscopy analyses point to a high degree of structural disorder of the BOS films. It manifests itself in a large width of reflexes on the XRD patterns (Fig. 1e) and presence of a wide background signal in the Raman spectra (Fig. 1f). The presence of wide background is typical for disordered semiconductors and related to the relaxation of the fundamental selection rule $k = 0$ (k is the wave-vector of a phonon) for one-phonon Raman scattering processes [32]. Identity of the XRD patterns and Raman spectra measured before and after heat treatment of the BOS films demonstrates the conservation of their phase composition.

3.4. Humidity sensing

To establish the possibility of formation of humidity sensors based on the BOS films, the following sequence of measurements was realized. The BOS film was placed in a darkened climate chamber and kept in the dark for half an hour before the start of the experiment. Then, the chamber was evacuated for 200 s. Further, water vapor was admitted for 700 s, after which the source of water vapor was disconnected from the chamber and it was pumped out for 200 s. The RH before the puffing was equal to 5%. The "puffing-pumping" cycle was repeated several times. The corresponding kinetics of the current changes (chronoamperogram) is shown in Fig. 5. Its analysis enables one to draw the following conclusions:

1. The puffing of water vapor leads to a sharp (up to three orders of magnitude) decrease in the resistance of the films.

2. The dependence of the current on time after the puffing of water vapor has a non-monotonic character: after a fast and sharp initial current increase, it slightly and slowly decreases with reaching a stationary value.

3. When cycling "puffing-pumping", the qualitative dependence of the current on time is preserved, however, there are noticeable differences in the stationary values of the current when the maximum and minimum values of the relative humidity are reached.

The small inertia of the prepared sensing structure attracts attention. Figure 6 demonstrates parts of the chronoamperogram corresponding to a change in the current immediately after the start of the puffing and pumping out water vapor. As can be seen from Fig. 6, the current increases by more than an order of magnitude within a second after the start of puffing. The recovery of the film resistance after the start of pumping out also occurs quite quickly: during the first second, the current decreases down to 10% of the stationary value reached at the maximum humidity.

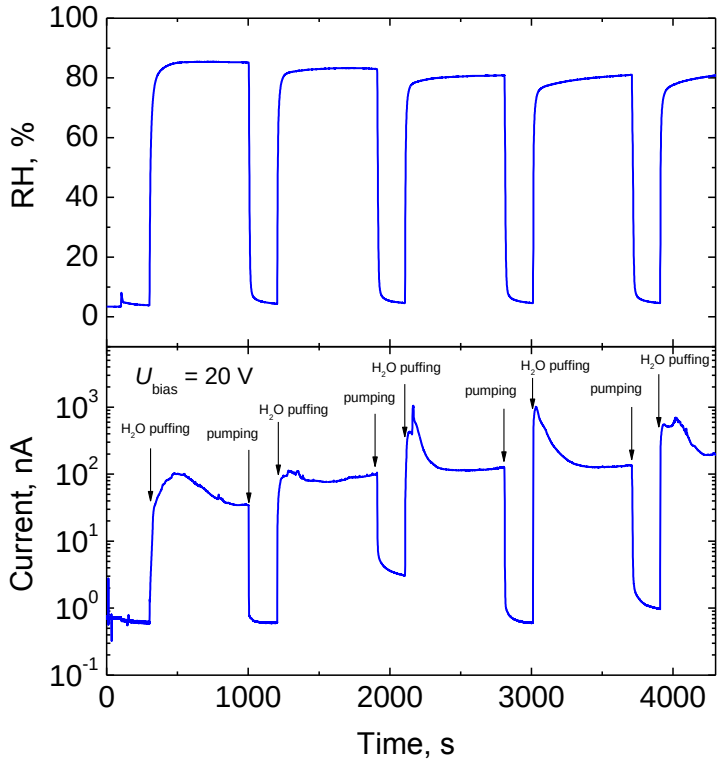

Fig. 5. Kinetics of the current changes for BOS film recorded under a constant bias voltage and cycling “puffing-pumping” of water vapor.

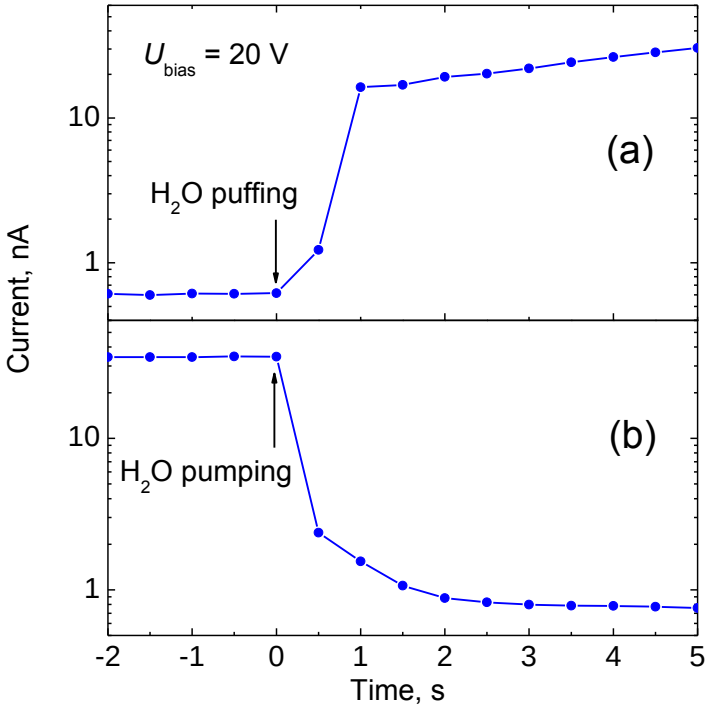

Fig. 6. Parts of kinetics of the current changes presented in Fig. 5 corresponding to start of water vapor puffing (a) and pumping (b).

There are many publications devoted to the creation of humidity sensors based on nanostructured metal chalcogenides and oxides [15–19, 33–35]. Most of the above resistive sensors have a long response/recovery times and a large hysteresis observed on the kinetics of sensors' resistance change during water adsoprption/desorption processes. One of the best results for devices based on bismuth compounds is presented in the article [19], which describes optimized relative humidity sensors based on Bi_2S_3 nanobelts. The described sensors have a fast response/recovery times in wet environments, good property reproducibility, and high stability. At the same time, the increase in current observed in [19] with an increase in humidity up to 90% was only about 13 times, while the presented in this paper BOS based sensing structure demonstrates an increase in current up to three orders of magnitude.

The noted non-monotonic dependence of current on RH points to existence of at least two opposite mechanisms of influence of adsorbed water on the BOS film resistivity. In general case, water adsorption can affect the resistivity by (i) change of the charge carriers concentration in semiconductor due to electron exchange with adsorbed water and species dissolved in it (first of all, molecular oxygen); (ii) ionic conductivity provided by adsorbed water.

A typical example of impact of electron accepting from semiconductor by the adsorbed water is described in work [33] for single layer MoS_2 film. Such process was confirmed experimentally by the photoluminescence spectroscopy (increase in the intensities ratio for the lines corresponding to neutral and negatively charged excitons with RH) and resulted in resistivity growth for MoS_2 films by four orders of magnitude upon RH increase from 0 to 35%. Note that despite the fact that in our case effect of RH change on resistivity is not so high, the BOS films reveal much shorter response to RH change in comparison with [33].

Taking into account the aforesaid, we suppose that the fast initial growth of current after H_2O puffing is influenced by dissociation of adsorbed water molecules, which results in appearance of ionic conductivity. This ionic conductivity is influenced mainly by hydroxide anions, whereas the protons are captured by oxygen and sulfur anions in BOS. Formation of O–H and S–H covalent bonds occurs according to the donor-acceptor mechanism due to the electron pairs of sulfur and oxygen. Moreover, a slight BOS dissolution (hydrated Bi^{3+} cations, HS^- and S^{2-} anions) can give some contribution into ionic

conductivity. Subsequent slow decrease of the current is determined by accepting electrons from *n*-type film by the oxygen dissolved in adsorbed water. Since the solubility of oxygen in water is rather low, the rate of this process is limited by the transfer of O_2 to the "water-BOS" interface.

The noted competition of the processes described above can probably explain diversity in effect of RH change on resistivity of semiconductor films. For example, in the afore-cited work [33] and work [34] the resistivity increase with RH was observed for MoS_2 and rGO:MoS_2 films, respectively. At the same time, in work [35] an opposite effect (conductivity increase by 6 orders of magnitude upon relative humidity increase from 10 to 95%) was observed for aerosol-printed MoS_2 films. It is reasonable to suppose that at low RH values ionic conductivity is impossible due to the absence of percolation aqueous solution cluster, and dominating mechanism of water adsorption is associated with electron acceptance from semiconductor, which gives rise to resistivity increase for *n*-type material. On the contrary, at rather high RH values, infinite percolation cluster of H_2O molecules is formed on the surface of the plate crystals inside of the film, which provides ionic conductivity and manifests itself as decrease of the film resistance.

4. Conclusions

In-plane electron transport properties of the BOS films prepared by the chemical bath deposition on dielectric glass substrates were studied. It was established that the as-prepared BOS films possess the dark resistivity of $3 \cdot 10^5$ Ω·cm. Heat treatment of the films at 200 °C in vacuum does not change their phase composition, but results in slowly (a few month) reversible decrease of the dark resistance by 7 orders of magnitude. Such behavior is explained by formation of anion vacancies during annealing, which leads to the increase of donor centers concentration in the films. The capture of oxygen from atmosphere during subsequent storage leads to an opposite effect. The BOS films have rather low photoconductivity under visible light illumination (several orders less than for liquid junction), which is due to charge carriers recombination and scattering at the interfaces between the nanoplates. BOS films demonstrate fast (several seconds) response to RH change, as well as high sensitivity (increase of current up to three orders of magnitude at a constant applied voltage when RH increases from 5 to 85%). Low photoconductivity of BOS films provides an additional selectivity of RH sensing even under illumination.

Acknowledgments

I.A.S., L.S.K., E.A.S., and A.V.M. acknowledge the Research Program "Photonics and Electronics for Innovations" of the Republic of Belarus for financial support. V.K.K. acknowledges the Research Program "Convergence-2025" of the Republic of Belarus for financial support. E.A.B. acknowledges the Polish National Centre for Research and Development, grant No SzN/I/30/Gigakwant/2022. A.V.M. expresses gratitude to Academician N.A. Poklonski and Professor N.M. Kazuchits for helpful discussions. The authors are grateful to Dr. A.I. Kovalev and Dr. D.V. Adamchuk for their help in implementation of humidity sensing experiments.

References

[1] Zimin Li, Ye Tian, Nano-bismuth-sulfide for advanced optoelectronics, Photonics 9 (2022) 790. https://doi.org/10.3390/photonics9110790.

[2] Taotao Ding, Jiangnan Dai, Juan Xu, Jin Wang, Wu Tian, Kaifu Huo, Yanyan Fang, Changqing Chen, 2015. 3D hierarchical Bi_2S_3 nanostructures by polyvinylpyrrolidone (PVP) and chloride ion-assisted synthesis and their photodetecting properties. Nanoscale Res. Lett. 10, 286. https://doi.org/10.1186/s11671-015-0993-1.

[3] Taotao Ding, Yu Tian, Jiangnan Dai, Changqing Chen, Building one-dimensional Bi_2S_3 nanorods as enhanced photoresponding materials for photodetectors, Front. Optoelectron. 8 (2015) 282–288. https://doi.org/10.1007/s12200-015-0529-4.

[4] Farid Jamali-Sheini, Mohsen Cheraghizade, Ladan Heshmatynezhad, An efficient wide range photodetector fabricated using a bilayer Bi_2S_3/SnS heterojunction thin film, Semicond. Sci. Technol. 34 (2019) 045008. https://doi.org/10.1088/1361-6641/ab0723.

[5] Mohd Shkir, Amira Ben Gouider Trabelsi, Fatemah H. Alkallas, Salem AlFaify, Bidhan Pandit, Mohd Ubaidullah, Improved optoelectronic properties of nanostructured Eu doped Bi_2S_3 thin films for the detection of UV light, Crystals 12 (2022) 1329. https://doi.org/10.3390/cryst12101329.

[6] Guihuan Chen, Yongqiang Yu, Kun Zheng, Tao Ding, Wenliang Wang, Yang Jiang, Qing Yang, Fabrication of ultrathin Bi_2S_3 nanosheets for high-performance, flexible, visible–NIR photodetectors, Small 11 (2015) 2848–2855. https://doi.org/10.1002/smll.201403508.

[7] Basant Chitara, Bhargava S.C. Kolli, Fei Yan, Near-infrared photodetectors based on 2D Bi_2S_3, Chem. Phys. Lett. 804 (2022) 139876. https://doi.org/10.1016/j.cplett.2022.139876.

[8] Jinzhuo Xu, Henan Li, Shaofan Fang, Ke Jiang, Huizhen Yao, Feier Fang, Fuming Chen, Ye Wang, Yumeng Shi, Synthesis of bismuth sulfide nanobelts for high performance broadband photodetector, J. Mater. Chem. C 8 (2020) 2102–2108. https://doi.org/10.1039/x0xx00000x.

[9] G. Zhang, Q. Zhang, Q. Hu, B. Wang, W. Yang, Giant enhancements in electronic transport and photoelectric properties of bismuth oxysulfide by pressure-driven 2D–3D structural reconstruction, J. Mater. Chem. A 7 (2019) 4019–4025. https://doi.org/10.1039/C8TA11168E.

[10] Xuxuan Yang, Lihang Qu, Feng Gao, Yunxia Hu, Huan Yu, Yunxia Wang, Mengqi Cui, Yunxiao Zhang, Zhendong Fu, Yuewu Huang, Wei Feng, Bin Li, PingAn Hu, High-performance broadband photoelectrochemical photodetectors based on ultrathin Bi_2O_2S nanosheets, ACS Appl. Mater. Interfaces 14 (2022) 7175−7183. https://doi.org/10.1021/acsami.1c22448.

[11] Sidra Farooq, Thomas Feeney, Joao O. Mendes, Vaishnavi Krishnamurthi, Sumeet Walia, Enrico Della Gaspera, Joel van Embden, High gain solution-processed carbon-free BiSI chalcohalide thin film photodetectors, Adv. Funct. Mater. 31 (2021) 2104788. https://doi.org/10.1002/adfm.202104788.

[12] Xiu Yan, Wei-Li Zhen, Hui-Jie Hu, Li Pi, Chang-Jin Zhang, Wen-Ka Zhu, High-performance visible light photodetector based on BiSeI single crystal, Chin. Phys. Lett. 38 (2021) 068103. https://doi.org/10.1088/0256-307X/38/6/068103.

[13] R.A. Jagt, T.N. Huq, K.M. Börsig, D. Sauven, L.C. Lee, J.L. MacManus-Driscoll, R.L.Z. Hoye, Controlling the preferred orientation of layered BiOI solar absorbers, J. Mater. Chem. C 8 (2020) 10791–10797. https://doi.org/10.1039/D0TC02076A.

[14] Wei Zeng, Jie Li, Liping Feng, Haixi Pan, Xiaodong Zhang, Hanqing Sun, Zhengtang Liu, Synthesis of large-area atomically thin BiOI crystals with highly sensitive and controllable photodetection, Adv. Funct. Mater. 29 (2019) 1900129. https://doi.org/10.1002/adfm.201900129.

[15] P.M. Faia, C.S. Furtado, A.J. Ferreira, Humidity sensing properties of a thick-film titania prepared by a slow spinning process, Sensors and Actuators B 101 (2004) 183–190. https://doi.org/10.1016/j.snb.2004.02.050.

[16] D.V. Adamchuck, V.K. Ksenevich, N.A. Poklonski, A.I. Kavaleu, Features of water vapor adsorption and desorption on the surface of non-stoichiometric tin dioxide films (in Russian), Proceedings of the National Academy of Sciences of Belarus. Physics and Mathematics Series 56 (2020) 102–113. https://doi.org/10.29235/1561-2430-2020-56-1-102-113.

[17] Y.P. Leung, Wallace C.H. Choy, T.I. Yuk, Linearly resistive humidity sensor based on quasi one-dimensional ZnSe nanostructures, Chem. Phys. Lett. 457 (2008) 198–201. https://doi.org/10.1016/j.cplett.2008.04.005.

[18] G. Kunakova, R. Meija, I. Bite, J. Prikulis, J. Kosmaca, J. Varghese, J.D. Holmes, Donats Erts, Sensing properties of assembled Bi_2S_3 nanowire arrays, Phys. Scr. 90 (2015) 094017. https://doi.org/10.1088/0031-8949/90/9/094017.

[19] Muhammad Faheem Afsar, M.A. Rafiq, Arifa Jamil, Sajid Fareed, Fizza Siddique, A.I.Y. Tok, Muhammad Masood ul Hasan, Development of high-performance bismuth sulfide nanobelts humidity sensor and effect of humid environment on its transport properties, ACS Omega 4 (2019) 2030−2039. https://doi.org/10.1021/acsomega.8b01854.

[20] Zhi Chen, Chi Lu, Humidity sensors: a review of materials and mechanisms, Sensor Lett. 3 (2005) 274–295. https://doi.org/10.1166/sl.2005.045.

[21] Hamid Farahani, Rahman Wagiran, Mohd Nizar Hamidon, Humidity sensors principle, mechanism, and fabrication technologies: a comprehensive review, Sensors 14 (2014) 7881–7939. https://doi.org/10.3390/s140507881.

[22] E.A. Bondarenko, E.A. Streltsov, M.V. Malashchonak, A.V. Mazanik, A.I. Kulak, E.V. Skorb, Giant incident photon-to-current conversion with photoconductivity gain on nanostructured bismuth oxysulfide photoelectrodes under visible-light illumination, Adv. Mater. 29 (2017) 1702387. https://doi.org/10.1002/adma.201702387.

[23] E.A. Bondarenko, E.A. Streltsov, A.V. Mazanik, A.I. Kulak, V. Grivickas, P. Ščajev, E.V. Skorb, Bismuth oxysulfide film electrodes with giant incident photon-to-current conversion efficiency: dynamics of properties with deposition time, Phys. Chem. Chem. Phys. 20 (2018) 20340–20346. https://doi.org/10.1039/C8CP03225D.

[24] E.A. Bondarenko, E.A. Streltsov, A.V. Mazanik, A.I. Kulak, Bismuth oxysulfide photoelectrodes with giant incident photon-to-current conversion efficiency: chemical stability in aqueous solutions, ChemElectroChem. 6 (2019) 2474–2481. https://doi.org/10.1002/celc.201900394.

[25] M.V. Malashchonak, A.V. Mazanik, O.V. Korolik, E.A. Streltsov, A.I. Kulak, Influence of wide band gap oxide substrates on the photoelectrochemical properties and structural disorder of CdS nanoparticles grown by the successive ionic layer adsorption and reaction (SILAR) method, Beilstein J. Nanotechnol. 6 (2015) 2252–2262. https://doi.org/10.3762/bjnano.6.231.

[26] E.A. Bondarenko, A.V. Mazanik, E.A. Streltsov, A.I. Kulak, O.V. Korolik, SnO_2 / Reduced graphene oxide composite films for electrochemical applications, Mater. Sci. Eng. B 202 (2015) 61–67. https://doi.org/10.1016/j.mseb.2015.10.002.

[27] M.E. Kazyrevich, M.V. Malashchonak, A.V. Mazanik, E.A. Streltsov, A.I. Kulak, C. Bhattacharya, Photocurrent switching effect on platelet-like BiOI electrodes: influence of redox system, light wavelength and thermal treatment, Electrochim. Acta 190 (2016) 612–619. https://doi.org/10.1016/j.electacta.2015.12.229.

[28] V. Grivickas, P. Ščajev, V. Bikbajevas, O.V. Korolik, A.V. Mazanik, Carrier dynamics in highly-excited $TlInS_2$: evidence of 2D-charge separation on layer interfaces, Phys. Chem. Chem. Phys. 21 (2019) 2102–2114. https://doi.org/10.1039/c8cp06209a.

[29] N.S. Mahon, O.V. Korolik, M.V. Khenkin, G.E. Arnaoutakis, Y. Galagan, V. Soriūtė, D. Litvinas, P. Ščajev, E.A. Katz, A.V. Mazanik, Photoluminescence kinetics for monitoring photoinduced processes in perovskite solar cells, Sol. Energy 195 (2020) 114–120. https://doi.org/10.1016/j.solener.2019.11.050.

[30] P. Grivickas, P. Ščajev, N. Kazuchits, S. Lastovskii, L.F. Voss, A.M. Conway, A. Mazanik, O. Korolik, V. Bikbajevas, V. Grivickas, Carrier recombination and diffusion in high-purity diamond after electron irradiation and annealing, Appl. Phys. Lett. 117 (2020) 242103. https://doi.org/10.1063/5.0028363.

[31] W.E. Taylor, N.H. Odell, H.Y. Fan, Grain boundary barriers in germanium, Phys. Rev. 38 (1952) 867–875. https://doi.org/10.1103/PhysRev.88.867.

[32] P.Y. Yu, M. Cardona, Fundamentals of Semiconductors: Physics and Materials Properties, fourth ed., Springer, Berlin, 2010.

[33] Jing Zhao, Na Li, Hua Yu, Zheng Wei, Mengzhou Liao, Peng Chen, Shuopei Wang, Dongxia Shi, Qijun Sun, Guangyu Zhang, Highly sensitive MoS_2 humidity sensors array for noncontact sensation, Adv. Mater. 29 (2017) 1702076. https://doi.org/10.1002/adma.201702076.

[34] Md Ridwan Adib, Yongbum Lee, Vijay V. Kondalkar, Sihyeok Kim, Keekeun Le, A highly sensitive and stable rGO:MoS_2-based chemiresistive humidity sensor directly insertable to transformer insulating oil analyzed by customized electronic sensor interface, ACS Sens. 6 (2021) 1012−1021. https://doi.org/10.1021/acssensors.0c02219.

[35] N.M. Pereira, N.P. Rezende, T.H.R. Cunha, A.P.M. Barboza, G.G. Silva, D. Lippross, B.R.A. Neves, H. Chacham, A.S. Ferlauto, R.G. Lacerda, Aerosol-printed MoS_2 ink as a high sensitivity humidity sensor, ACS Omega 7 (2022) 9388−9396. https://doi.org/10.1021/acsomega.1c06525.